CRYSTAL GROWTH & DESIGN

pubs.acs.org/crystal

Article

Stereochemical Control of Cocrystal and Hybrid Salt−Cocrystal Formation in the Baclofen−Mandelic Acid System

Published as part of Crystal Growth & Design special issue "Design of Crystals via Crystallization Processes".

Sarita Songsermsawad, Kajjana Boonpalit, Oleksii Shemchuk, Koen Robeyns, Tom Leyssens,* and Adrian E. Flood*

Cite This: *Cryst. Growth Des.* 2025, 25, 6830−6836

Read Online

ACCESS | Metrics & More | Article Recommendations | Supporting Information

ABSTRACT: Chiral resolution by crystallization is a highly scalable and economically viable technique crucial for the pharmaceutical industry. While the use of multicomponent crystals, such as salts and cocrystals, has been extensively explored for separating racemates, precisely controlling the solid form selection in systems with multiple possible interactions remains a significant challenge. This study investigates the mechanochemical and crystallization products resulting from various enantiomeric combinations of the chiral active pharmaceutical ingredient baclofen and mandelic acid. We reveal that combining enantiopure mandelic acid with racemic baclofen leads to chiral resolution through the formation of diastereomeric cocrystals. Conversely, combining racemic mandelic acid with baclofen produces solid solution hybrid salt−cocrystals, highlighting the diverse outcomes of specific enantiomeric pairings. The stability of multicomponent formations was complementarily studied by employing density functional theory to calculate the lattice energy of each form. These findings uniquely showcase how stereochemistry fundamentally governs both solid form selection and specific chiral recognition pathways at the molecular level, providing crucial insights into the rational design of advanced chiral separation strategies.

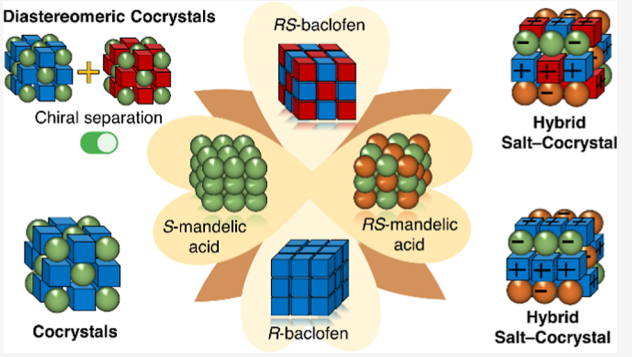

1. INTRODUCTION

Single-enantiomer drugs are in high demand due to their superior therapeutic efficacy and extended patentability.[1,2] Regulatory agencies such as the U.S. Food and Drug Administration (FDA) and the European Medicines Agency (EMA) increasingly favor the registration of enantiomerically pure forms.[3,4] Although enantiomers of active pharmaceutical ingredients (APIs) possess identical molecular formulas and exhibit identical physical properties in achiral environments, their behavior in chiral environments—such as those in biological systems—can differ markedly.[5] As a result, the development of the methods to achieve enantiopure compounds has become essential in pharmaceutical manufacturing.

A number of chiral resolution methods have been developed, such as asymmetric synthesis, chiral chromatography, adsorption, and membrane separations. Among various resolution techniques,[6] crystallization-based methods are particularly attractive due to their operational simplicity, cost effectiveness, and scalability.[7,8] However, a major challenge arises as most chiral compounds crystallize as racemic compounds[9] (consisting of equal amounts of the two enantiomers in the same crystal lattice), which makes their separation by conventional crystallization difficult.

Salts and cocrystals are the most commonly employed multicomponent solid forms in chiral resolution by crystallization.[10,11] A well-known classical technique is Pasteur's resolution,[12] which involves forming diastereomeric salts by combining a racemic mixture with a chiral resolving agent. Each enantiomer interacts differently with the resolving agent, yielding diastereomeric salt crystals with distinct physical properties that allow for separation. More recently, cocrystals have gained interest in pharmaceutical solid-state chemistry for their ability to modulate API properties without altering chemical structures.[13] Analogous to salts, cocrystals can also be used for chiral resolution: enantiomers interact differently with a chiral coformer, resulting in diastereomeric or enantiospecific cocrystals that can be separated by crystallization.[14]

Received: May 29, 2025
Revised: July 22, 2025
Accepted: July 23, 2025
Published: July 30, 2025

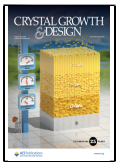

https://doi.org/10.1021/acs.cgd.5c00779
Cryst. Growth Des. 2025, 25, 6830−6836

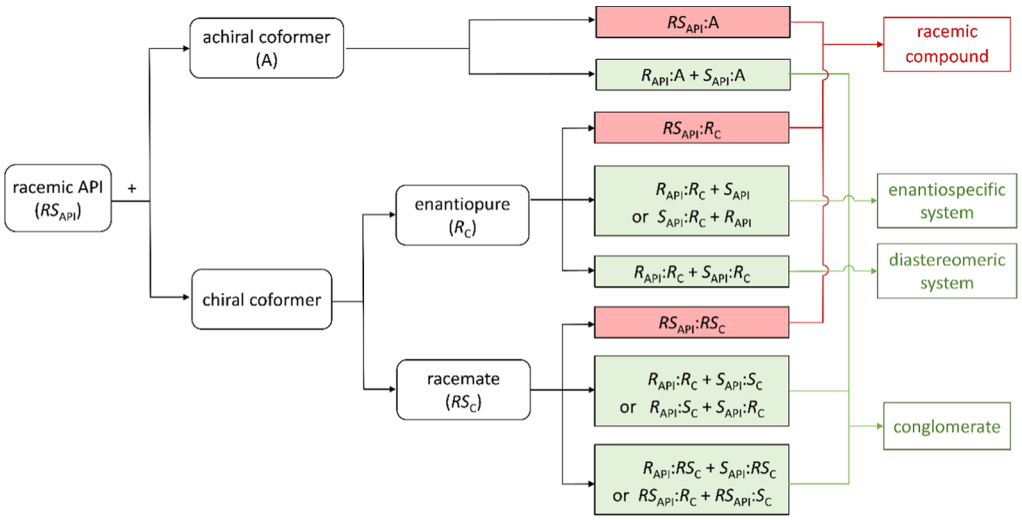

Figure 1. Potential outcomes when combining a racemic API (RS_{API}) with an achiral (A), enantiopure (R_C), or racemic (RS_C) coformer with green and red showing favorable or nonfavorable chiral resolution processes, respectively.

The primary distinction between salts and cocrystals lies in the nature of the intermolecular interactions in the crystal.[15] Salts are defined by ionic bonding interactions, whereas cocrystals involve hydrogen bonding, $\pi-\pi$ stacking, or other noncovalent interactions. A hybrid form, known as a salt−cocrystal also exists, with the solid form containing two or more components with nonzero total charges and one or more neutral coformers.[15]

The chirality of the coformer plays a critical role in determining the outcome of the multicomponent crystallization,[16−19] as summarized in Figure 1. When a selected coformer creates a multicomponent crystal with an API, various outcomes are possible including racemic, diastereomeric, enantiospecific, or conglomerate multicomponent crystals. For instance, an enantiopure coformer may form enantiospecific cocrystals[20−25] (with only one enantiomer of the API) or diastereomeric cocrystals[26−35] (with both enantiomers). These structures often enable resolution via simple crystallization, as the two forms have different solubilities. In contrast, when a racemic coformer or achiral compound is used, the desired outcome is a conglomerate,[18,36−45] which allows for simultaneous resolution of both the API and the coformer (if a racemic compound is used) through the use of preferential crystallization. However, if a racemic compound forms,[46−49] separation becomes impossible because the enantiomers remain within the same crystal lattice.

In our previous work,[32] we proposed a chiral resolution method for racemic baclofen (Bac), an API which treats spinal cord injury and spasticity, via the formation of diastereomeric cocrystals with enantiopure mandelic acid (Man). *R*-Bac is retrieved from solution by cocrystallization with *S*-Man. Here, we present a complete study of the stereochemical recognition of the chiral−chiral system of Bac and Man, demonstrating how chiral configurations govern the formation of diverse multicomponent crystals. Also, density functional theory was utilized to calculate the lattice energy of the system to emphasize the thermodynamic formation of the multicomponent solid.

2. EXPERIMENTAL SECTION

2.1. Starting Materials. *RS*-Bac (≥98.0%), *RS*-Man (>99.0%), *R*-Man (>99.0%), and *S*-Man (>98.0%) were purchased from Tokyo Chemical Industry Co. (TCI). Acetic acid (Glacial, 99.8%) was purchased from Merck. Ultrapure water type I (18.2 MΩ) was obtained from PURELAB Classic (ELGA). *R*-Bac (94.5% enantiomeric excess) was resolved from *RS*-Bac using a method adapted from our previous work.[32] The details are given in Supporting Information.

2.2. Grinding Experiment. Liquid-assisted grinding (LAG) was performed to screen multicomponent formation of combinations with different chiral configurations of Bac and Man using a RETSCH Mixer Mill (MM200) in a 2 mL plastic tube with 3 7 mm stainless steel-balls. A 150 mg mixture of Bac and Man was prepared before grinding with 10 μL of methanol for 1.5 h with a frequency of 25 Hz. Five different experiments were tested, with each having a unique chiral combination. All of the enantiomeric combinations between two chiral compounds are shown in eq 1−5. Equations 1 and 2 are enantiopure−enantiopure interactions, which refer to the combination of enantiopure components of the two compounds. Equations 3−5 are tested to explore the potential of enantiospecific or diastereomeric cocrystal chiral resolution of either Bac (**3**) or Man (**4**), and the potential to find a conglomerate cocrystal (**5**). The two sides of each equation show stereoisomers that have identical stability. Therefore, grinding only one of the two identical combinations from eqs 1−4 was sufficient. After grinding, the samples were dried under ambient conditions for 24 h and then were characterized by powder X-ray diffraction (XRPD) on a Bruker D8 Advance powder X-ray diffractometer equipped with a Cu Kα X-ray source (λ = 1.5406 Å) operating at 40 kV and 30 mA. The data were collected within 2θ values from 6° to 35° at a scan rate of 12° min^{-1}. The XRPD patterns of the samples were compared to the reactants.

$$R\text{-Bac} + R\text{-Man} = S\text{-Bac} + S\text{-Man} \quad (1)$$

$$R\text{-Bac} + S\text{-Man} = S\text{-Bac} + R\text{-Man} \quad (2)$$

$$RS\text{-Bac} + R\text{-Man} = RS\text{-Bac} + S\text{-Man} \quad (3)$$

$$R\text{-Bac} + RS\text{-Man} = S\text{-Man} + RS\text{-Man} \quad (4)$$

$$RS\text{-Bac} + RS\text{-Man} \quad (5)$$

2.3. Thermal Analysis. Thermogravimetric analysis (TGA) and differential scanning calorimetry (DSC) were performed to investigate the thermal behavior of the powder samples. TGA measurement was performed using a Thermal Plus Evo2 (TG 8121, Rigaku) under a nitrogen (N_2) atmosphere at the flow rate of 200 cm^3 min^{-1}. Powder samples of 5 to 10 mg were prepared in aluminum pan heating from 30 to 250 °C with the ramping rate of 10 °C min^{-1} to measure the decomposition temperature. DSC was performed with a DSC8500 instrument (PerkinElmer). Powder samples of 5 to 10 mg were placed

https://doi.org/10.1021/acs.cgd.5c00779
Cryst. Growth Des. 2025, 25, 6830−6836

in an aluminum pan and cover. Samples were heated from 30 to 160 °C or to the decomposition temperature at a 5 °C min^{-1} heating rate.

2.4. Crystal Structure Determination. 1:2 *R*-Bac:*RS*-Man and 1:2 *RS*-Bac:*RS*-Man crystals were obtained from evaporative crystallization of solutions of *R*-Bac + *RS*-Man and *RS*-Bac + *RS*-Man combinations in water. Bac and Man were added in amounts close to their solubilities, and the solvents were then evaporated under ambient conditions until crystallization occurred. Details on crystallization conditions of each crystal are provided in Supporting Information. Single crystals were harvested from the solutions for the structure determination. Diffraction data were collected on a MAR345 image plate using MoKα radiation generated by an Incoatec IμS microfocus source (Montel Mirrors). Data reduction was carried out using the CrysAlis^{PRO} software package.[50] The resolution and refinement by full-matrix least-squares were carried out using respectively SHELXT[51] and SHELX-2018/3.[52] Non-hydrogen atoms were refined anisotropically; H atoms were added in calculated positions and allowed to ride on the parent atoms, with isotropic displacement factors set to 1.2 equiv of the parent atoms (Uiso(H) = 1.5Ueq(C) for methyl to OH hydrogens). For the structures showing disorder, the disorder presents itself as *R*/*S* disorder where both enantiomers are superposed onto each other, while maintaining the same hydrogen bond interactions. Isotropic and rigid bond restraints were set up for all atoms of the minor part, and the minor component was geometrically refined to be similar to the main component and occupancies were freely refined.

2.5. Density Functional Theory (DFT) Calculation. All first-principles calculations were conducted using the Vienna Ab initio Simulation Package[53,54] (VASP). Spin-polarized density functional theory (DFT) calculations employed the Perdew–Burke–Ernzerhof[55] (PBE) generalized gradient approximation (GGA) exchange–correlation functional with many-body dispersion[56,57] (MBD) corrections, PBE–MBD, in conjunction with the projector augmented wave[58] (PAW) method. The plane-wave cutoff energy of 520 eV, the energy convergence threshold of 10^{-5} eV, and the force convergence threshold of 0.02 eV $Å^{-1}$ were applied. Gaussian smearing with a width of 0.05 eV was utilized. The Brillouin zone sampling was performed using a 3 × 3 × 3 Monkhorst–Pack k-point mesh.

The calculation of Helmholtz free energy $F(T)$ was performed in order to include temperature effects at 300 K

$$F(T) = E_{total} + F_{vib}(T) \quad (6)$$

where E_{total} is the total energy, $F_{vib}(T)$ is the vibrational free energy, and T is the temperature. The calculation of Helmholtz free energy of molecular crystals and isolated molecules was performed using the CrystalThermo and HarmonicThermo utility within the Atomic Simulation Environment[59] (ASE) thermochemistry package, respectively. To obtain vibrational frequencies, numerical calculations were conducted via finite-difference methods with atomic displacements of 0.005 Å.[60,61] The lattice free energy (ΔF_{latt}) of a cocrystal, representing thermodynamic stability, is defined as

$$\Delta F_{latt} = (F_{crystal} - \sum_i x_i F_{mol,i})/n \quad (7)$$

where $F_{crystal}$ is the free energy of the molecular crystal, $F_{mol,i}$ is free energy of isolated molecule i forming the molecular crystal, x_i is the number of isolated molecule i in unit cell, n is the total number of molecules in the unit cell.

3. RESULT AND DISCUSSION

3.1. Multicomponent Products from Different Chiral Combinations of Bac and Man. Each unique chiral combination of Bac and Man results in a distinct multicomponent solid form. This is consistent with previous findings[16−19] that stereochemistry plays a critical role in solid-state assembly. The different stereochemical pairings between Bac and Man significantly influenced the outcome of the mechanochemical multicomponent products, as shown in Figure 2. XRPD patterns obtained from grinding 1:1 stoichiometric ratio *R*-Bac + *R*-Man (**1**) and *R*-Bac + *S*-Man

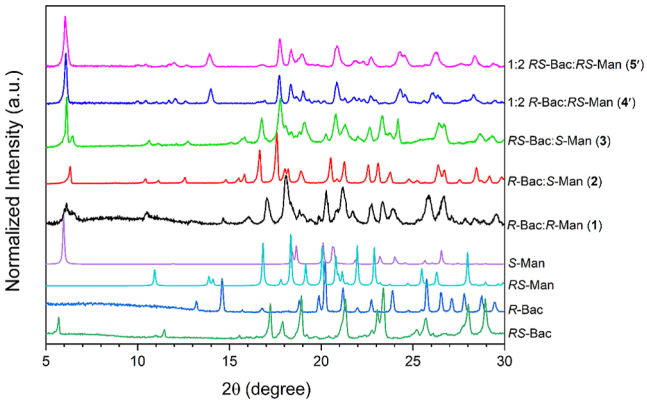

Figure 2. XRPD patterns of different chiral combinations between Bac and Man with 1:1 stoichiometric ratio of *R*-Bac:*R*-Man (**1**), *R*-Bac:*S*-Man (**2**), and *RS*-Bac:*S*-Man (**3**) and 1:2 stoichiometric ratio of *R*-Bac:*RS*-Man (**4′**) and *RS*-Bac:*RS*-Man (**5′**).

(**2**) systems were distinct from each other and from those of the starting materials, confirming the formation of new crystalline phases. Also, the pattern of 1:1 *RS*-Bac + *R*-Man (**3**) was a mixture of the prior two combinations (**1**) and (**2**), indicating that racemic Bac dissociates to form diastereomeric cocrystals with *R*-Man (*R*-Bac:*R*-Man + *S*-Bac:*R*-Man). These results were aligned with our previously published results[32] that enantiopure Man can resolve racemic Bac by forming diastereomeric cocrystals. The XRPD patterns of both 1:1 *R*-Bac + *RS*-Man (**4**) and 1:1 *RS*-Bac + *RS*-Man (**5**) show a mixture of the crystalline phase and residual Bac, indicating an incomplete transformation at a 1:1 stoichiometric ratio (Figure S1). This suggests that the reaction needs more Man to completely transform to the new phase. Therefore, the grinding experiments were repeated with a 1:2 stoichiometric ratio of Bac/Man for systems **4** (**4′**) and **5** (**5′**). Interestingly, both **4′** and **5′** produced complete conversion with the resulting powders showing nearly identical XRPD patterns (Figure 2), suggesting formation of a structurally similar phase that did not correspond to any of the known diastereomeric cocrystals of Bac-Man. The combination **5′** may represent either a mixture of two mirror-equivalent forms of **4′** (a conglomerate of the racemic cocrystal), which would be beneficial for chiral resolution, or a single racemic–racemic cocrystal structurally identical to **4′**, which would hamper resolution. Further structural analysis allowed characterization of these forms, especially **5′**.

3.2. Crystal Structure Analysis. To truly confirm the new crystalline phases from combinations **4′** and **5′**, their crystal structures were examined by using SC-XRD analysis of crystals harvested from those combinations. The crystallographic details of each structure are summarized in Table 1. The crystal structures of **4′** and **5′** exhibited highly similar unit cell parameters, explaining their comparable XRPD patterns. The asymmetric units of both crystal structures, shown in Figure 3 contain three species: protonated Bac (Bac^+), deprotonated Man (Man^-), and neutral Man, consistent with the definition of a salt-cocrystal[15] with a 1:2 molar ratio between Bac and Man.

Both **4′** and **5′** have near identical packing arrangements and can be superposed easily (Figure 4). With structure **4′** as the

https://doi.org/10.1021/acs.cgd.5c00779
Cryst. Growth Des. 2025, 25, 6830−6836

Table 1. Crystallographic Data of Hybrid Salt−Cocrystals

crystal data	1:2 *R*-Bac:*RS*-Man (**4′**)	1:2 *RS*-Bac:*RS*-Man (**5′**)
CSD number	2454488	2454489
species	2*R*-Bac$^+$:*R*-Man$^-$:*S*-Man$^-$:*R*-Man:*S*-Man	*R*-Bac$^+$:*S*-Bac$^+$:*R*-Man$^-$:*S*-Man$^-$:*R*-Man:*S*-Man
formula	$C_{10}H_{13}ClNO_2$, $C_8H_7O_3$, $C_8H_8O_3$	$C_{10}H_{13}ClNO_2$, $C_8H_7O_3$, $C_8H_8O_3$
temperature (K)	297	297
crystal system	triclinic	triclinic
space group	*P*1	$P\bar{1}$
a (Å)	9.1623(8)	9.2060(11)
b (Å)	10.3191(10)	10.2479(15)
c (Å)	15.2403(19)	15.310(2)
α (deg)	74.231(10)	74.528(13)
β (deg)	83.910(9)	84.985(11)
γ (deg)	68.507(9)	67.951(12)
volume (Å^3)	1290.23	1290.1
Z	2	2
R_1 ($I \geq 2\sigma(I)$)	0.0437	0.0660
wR_2 (all data)	0.1120	0.1759

reference point, **5′** can be seen as a solid solution where the enantiopure *R*-Bac in **4′** is substituted by a racemic mixture of *R*- and *S*-Bac on the same crystallographic position. As can be seen in Figure 4, the enantiopure Bac in **4′** always superposes with one of the disordered *R*/*S*-Bac molecules of **5′**. This also implies the observed pseudoinversion center in structure **4′**, while containing only enantiopure *R*-Bac.

The structural comparison between hybrid salt−cocrystals **4′** and **5′** and a cocrystal of *R*-Bac:*S*-Man, **2** reveals differences in both the stoichiometry and the nature of intermolecular interactions. In the crystal structure of **2** (CSD refcode: BAWNUM), the *R*-Bac molecule exists in its zwitterionic form and *S*-Man remains in its neutral form. The packing in the structure is created mainly by hydrogen bonding between acid−base heterosynthons and by layer stacking through the halogen-*π* interaction of the chlorine of Bac and the phenyl ring of Man. The ΔpK_a between Bac and Man is approximately 0.5 (pK_a values: Bac = 3.87;[62] Man = 3.41[63]), placing the system near the intermediate zone where both salt, cocrystal, or hybrid formation are possible. Notably, hybrid salt−cocrystals were observed to form depending on the chiral configuration of the components, implying that chirality may play a role in controlling the assembly and molecular recognition within the solid-state structure.

Crystallization with the **1** combination resulted in an oil droplet, potentially due to compound decomposition, thus preventing structural determination of this form.

3.3. Thermal Analysis. Thermal behavior of each multicomponent crystal (both cocrystal and salt−cocrystal) were evaluated using TGA and DSC, as summarized in Table 2. All crystal forms except **1** melted at their decomposition temperature of around 130 °C showing the first stage of weight loss up to 170 °C. The 1:1 cocrystal and the 1:2 hybrid salt−cocrystal exhibited 5% and 4% weight loss (see Supporting Information), likely due to surface water or the dehydration reaction of baclofen to form 4-(4-chlorophenyl)-2-pyrrolidone.[64] **1** has the lowest melting temperature and **2** has the highest decomposition temperature among the others. Since a higher melting and decomposition temperature often suggests greater stability, **2** could be the most stable multicomponent crystal form. However, the direct comparison should account for differences in overall composition.

3.4. DFT Calculation. In this section, we performed DFT calculations to theoretically validate the thermodynamic stability of cocrystals, confirming that *RS*-Bac spontaneously resolves into individual enantiomers when crystallizing with *R*- or *S*-Man, while *RS*-Man combines with *RS*-Bac without enantiomeric separation. All DFT calculations employ the PBE−MBD functional because it offers both computational cost-effectiveness and comparable accuracy to the computationally demanding PBE0−MBD functional, which serves as the benchmark standard for molecular crystal systems.[60,65,66] The calculated energies are shown in Table S1.

The lattice free energies (ΔF_{latt}) show that **5′** exhibits the most favorable value at −34.383 kcal mol^{-1}, followed closely by **4′** at −34.291 kcal mol^{-1}, with only a minimal difference between them. This extremely small free energy difference indicates that *RS*-Man shows analogous interaction and similar thermodynamic stability when forming cocrystals with either *RS*-Bac or *R*-Bac alone, explaining why *RS*-Man does not promote enantiomeric resolution during cocrystallization since there is no thermodynamic preference driving chiral discrimination.

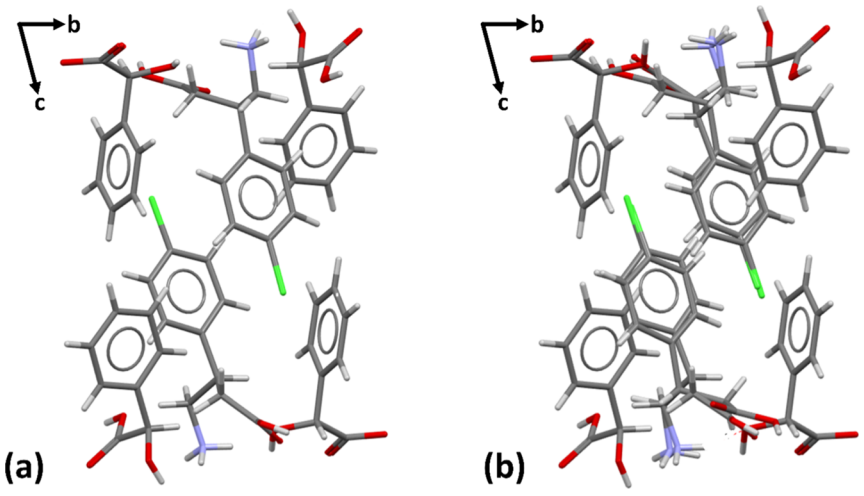

Figure 3. Unit cell of hybrid salt−cocrystals (a) **4′** and (b) **5′**.

https://doi.org/10.1021/acs.cgd.5c00779
Cryst. Growth Des. 2025, 25, 6830−6836

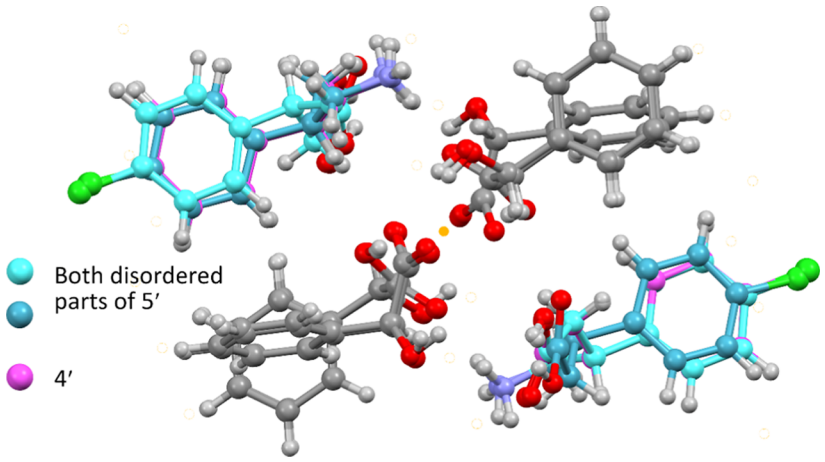

Figure 4. Overlay of structure **4′** and **5′**, the enantiopure Bac in **4′** (magenta) superposes with one of the disordered parts of **5′** (top left vs bottom right). The (pseudo)-inversion center is indicated with an orange dot.

Table 2. Thermal Data of Cocrystals and Salt−Cocrystals Obtained From DSC and TGA

multicomponent crystal	decomposition temperature (°C)	melting temperature (°C)
R-Bac:*R*-Man (**1**) cocrystal	117	89
R-Bac:*S*-Man (**2**) cocrystal	131	melting followed by decomposition
1:2 *R*-Bac:*RS*-Man (**4′**) hybrid salt−cocrystal	126	melting followed by decomposition
1:2 *RS*-Bac:*RS*-Man (**5′**) hybrid salt−cocrystal	129	melting followed by decomposition

Notably, the **2** system with enantiopure *S*-Man displays a less favorable ΔF_{latt} of −33.023 kcal mol^{-1}, which is 1.384 kcal mol^{-1} higher than that of the racemic *RS*-Man systems. This reduced thermodynamic favorability suggests that while enantiopure *S*-Man and *R*-Bac combinations are viable, they are not as energetically preferred as the *RS*-Man systems. The computational findings align with the experimental results, indicating that *RS*-Bac undergoes enantiomeric resolution exclusively when crystallized with *S*-Man.

4. CONCLUSIONS

This work demonstrates that chiral resolution of both components simultaneously cannot be achieved in the system of racemic Bac and racemic Man, despite the fact that a specific chiral combination (e.g., enantiopure Man with racemic Bac) successfully forms diastereomeric cocrystals that allow for resolution by solubility differences. Moreover, the study also reveals that not only the chemical identity but also the stoichiometry and chiral configuration of the components play critical roles in determining the type of multicomponent formation. When enantiopure Man is used, a 1:1 cocrystal with Bac is formed. However, the presence of racemic Man results in the formation of a hybrid salt−cocrystal with a different stoichiometric ratio (1:2 Bac to Man). Lattice energy calculations using DFT support these observations, showing that the hybrid salt−cocrystal formed from racemates of both components is the most thermodynamically stable phase.

■ ASSOCIATED CONTENT

Supporting Information

The Supporting Information is available free of charge at https://pubs.acs.org/doi/10.1021/acs.cgd.5c00779.

Additional experimental details, XRPD patterns, and thermal analysis (PDF)

Accession Codes

Deposition Numbers 2454488−2454489 contain the supplementary crystallographic data for this paper. These data can be obtained free of charge via the joint Cambridge Crystallographic Data Centre (CCDC) and Fachinformationszentrum Karlsruhe.

■ AUTHOR INFORMATION

Corresponding Authors

Tom Leyssens − *Institute of Condensed Matter and Nanosciences, Université Catholique de Louvain, Louvain-La-Neuve 1348, Belgium;* orcid.org/0000-0001-7916-1373; Email: tom.leyssens@uclouvain.be

Adrian E. Flood − *School of Energy Science and Engineering, Vidyasirimedhi Institute of Science and Engineering, Rayong 21210, Thailand;* orcid.org/0000-0003-1691-3085; Email: adrian.flood@vistec.ac.th

Authors

Sarita Songsermsawad − *School of Energy Science and Engineering, Vidyasirimedhi Institute of Science and Engineering, Rayong 21210, Thailand*

Kajjana Boonpalit − *School of Information Science and Technology, Vidyasirimedhi Institute of Science and Engineering, Rayong 21210, Thailand;* orcid.org/0000-0002-9325-387X

Oleksii Shemchuk − *Institute of Condensed Matter and Nanosciences, Université Catholique de Louvain, Louvain-La-Neuve 1348, Belgium;* orcid.org/0000-0003-3003-3922

Koen Robeyns − *Institute of Condensed Matter and Nanosciences, Université Catholique de Louvain, Louvain-La-Neuve 1348, Belgium;* orcid.org/0000-0002-4763-4217

Complete contact information is available at: https://pubs.acs.org/10.1021/acs.cgd.5c00779

Author Contributions

The manuscript was written through contributions of all authors. All authors have given approval to the final version of the manuscript.

https://doi.org/10.1021/acs.cgd.5c00779
Cryst. Growth Des. 2025, 25, 6830−6836

Funding

S.S. was supported through a Postdoctoral scholarship from Vidyasirimedhi Institute of Science and Technology (VISTEC). S.S. and A.F. thank the Frontier Research Center of VISTEC for equipment support. K.B. was supported by a VISTEC-NSTDA collaborative research and education scholarship.

Notes

The authors declare no competing financial interest.

■ ACKNOWLEDGMENTS

The authors would like to thank the Vidyasirimedhi Institute of Science and Technology (VISTEC) for the Postdoctoral scholarship for S.S. K.B. was supported by a VISTEC-NSTDA collaborative research and education scholarship.

■ REFERENCES

(1) Calcaterra, A.; D'Acquarica, I. The market of chiral drugs: Chiral switches versus de novo enantiomerically pure compounds. *J. Pharm. Biomed. Anal.* **2018**, *147*, 323−340.
(2) Senkuttuvan, N.; Komarasamy, B.; Krishnamoorthy, R.; Sarkar, S.; Dhanasekaran, S.; Anaikutti, P. The significance of chirality in contemporary drug discovery-a mini review. *RSC Adv.* **2024**, *14* (45), 33429−33448.
(3) McVicker, R. U.; O'Boyle, N. M. Chirality of New Drug Approvals (2013−2022): Trends and Perspectives. *J. Med. Chem.* **2024**, *67* (4), 2305−2320.
(4) Bhutani, P.; Joshi, G.; Raja, N.; Bachhav, N.; Rajanna, P. K.; Bhutani, H.; Paul, A. T.; Kumar, R. U. S. FDA Approved Drugs from 2015−June 2020: A Perspective. *J. Med. Chem.* **2021**, *64* (5), 2339−2381.
(5) Chuong, P. H.; Nguyen, L. A.; He, H. Chiral drugs: an overview. *Int. J. Biomed. Sci.* **2006**, *2* (2), 85−100.
(6) Teng, Y.; Gu, C.; Chen, Z.; Jiang, H.; Xiong, Y.; Liu, D.; Xiao, D. Advances and applications of chiral resolution in pharmaceutical field. *Chirality* **2022**, *34* (8), 1094−1119.
(7) Lorenz, H.; Seidel-Morgenstern, A. Processes To Separate Enantiomers. *Angew. Chem., Int. Ed.* **2014**, *53* (5), 1218−1250.
(8) Mane, S. Racemic drug resolution: a comprehensive guide. *Anal. Methods* **2016**, *8* (42), 7567−7586.
(9) Jacques, J.; Collet, A.; Wilen, S. H.; Collet, A. *Enantiomers, Racemates, and Resolutions*; Wiley: New York, 1981.
(10) Grothe, E.; Meekes, H.; de Gelder, R. Chirality and stereoisomerism of organic multicomponent crystals in the CSD. *CrystEngComm* **2020**, *22* (43), 7380−7388.
(11) Scowen, I. J.; Alomar, T. S.; Munshi, T.; Seaton, C. C. Structural similarity in chiral-achiral multi-component crystals. *CrystEngComm* **2020**, *22* (43), 7334−7340.
(12) Vantomme, G.; Crassous, J. Pasteur and chirality: A story of how serendipity favors the prepared minds. *Chirality* **2021**, *33* (10), 597−601.
(13) Aitipamula, S.; Bolla, G. Optimizing Drug Development: Harnessing the Sustainability of Pharmaceutical Cocrystals. *Mol. Pharmaceutics* **2024**, *21* (7), 3121−3143.
(14) Kaviani, R.; Jouyban, A.; Shayanfar, A. Chiral resolution methods for racemic pharmaceuticals based on cocrystal formation. *CrystEngComm* **2023**, *25* (44), 6120−6131.
(15) Grothe, E.; Meekes, H.; Vlieg, E.; ter Horst, J. H.; de Gelder, R. Solvates, Salts, and Cocrystals: A Proposal for a Feasible Classification System. *Cryst. Growth Des.* **2016**, *16* (6), 3237−3243.
(16) Li, W.; de Groen, M.; Kramer, H. J. M.; de Gelder, R.; Tinnemans, P.; Meekes, H.; ter Horst, J. H. Screening Approach for Identifying Cocrystal Types and Resolution Opportunities in Complex Chiral Multicomponent Systems. *Cryst. Growth Des.* **2021**, *21* (1), 112−124.
(17) Zhou, F.; Body, C.; Robeyns, K.; Leyssens, T.; Shemchuk, O. On the pairwise cocrystallization of racemic compounds. *CrystEngComm* **2023**, *25* (20), 3060−3065.
(18) Songsermsawad, S.; Shemchuk, O.; Robeyns, K.; Collard, L.; Flood, A. E.; Leyssens, T. Simultaneously resolving BINOL and proline using a stoichiometric cocrystal switch. *Chem. Commun.* **2024**, *60* (52), 6607−6610.
(19) Rapeenun, P.; Songsermsawad, S.; Boonpalit, K.; Nalaoh, P.; Flood, A. E. Enhancing the Screening Efficiency of Chiral Cocrystals for the Separation of Praziquantel through the Use of Coformer Derivatives. *Cryst. Growth Des.* **2025**, *25* (3), 790−800.
(20) Springuel, G.; Leyssens, T. Innovative Chiral Resolution Using Enantiospecific Co-Crystallization in Solution. *Cryst. Growth Des.* **2012**, *12* (7), 3374−3378.
(21) Hu, X.; Shan, Z.; Chang, Q. An improved and practical approach to essentially enantiopure BINOLs: enantioselective inclusion complexation of (S)-proline. *Tetrahedron: Asymmetry* **2012**, *23* (18), 1327−1331.
(22) Harmsen, B.; Leyssens, T. Enabling enantiopurity: Combining racemization and dual-drug co-crystal resolution. *Cryst. Growth Des.* **2018**, *18* (6), 3654−3660.
(23) Harmsen, B.; Leyssens, T. Dual-Drug Chiral Resolution: Enantiospecific Cocrystallization of (S)-Ibuprofen Using Levetiracetam. *Cryst. Growth Des.* **2018**, *18* (1), 441−448.
(24) Nulek, T.; Klaysri, R.; Cedeno, R.; Nalaoh, P.; Bureekaew, S.; Promarak, V.; Flood, A. E. Separation of Etiracetam Enantiomers Using Enantiospecific Cocrystallization with 2-Chloromandelic Acid. *ACS Omega* **2022**, *7* (23), 19465−19473.
(25) Wang, J.; Peng, Y. Resolution of Halogenated Mandelic Acids through Enantiospecific Co-Crystallization with Levetiracetam. *Molecules* **2021**, *26* (18), 5536.
(26) Springuel, G.; Robeyns, K.; Norberg, B.; Wouters, J.; Leyssens, T. Cocrystal Formation between Chiral Compounds: How Cocrystals Differ from Salts. *Cryst. Growth Des.* **2014**, *14* (8), 3996−4004.
(27) Eddleston, M. D.; Arhangelskis, M.; Friščić, T.; Jones, W. Solid state grinding as a tool to aid enantiomeric resolution by cocrystallisation. *Chem. Commun.* **2012**, *48* (92), 11340−11342.
(28) Sánchez-Guadarrama, O.; Mendoza-Navarro, F.; Cedillo-Cruz, A.; Jung-Cook, H.; Arenas-García, J. I.; Delgado-Díaz, A.; Herrera-Ruiz, D.; Morales-Rojas, H.; Höpfl, H. Chiral Resolution of RS-Praziquantel via Diastereomeric Co-Crystal Pair Formation with l-Malic Acid. *Cryst. Growth Des.* **2016**, *16* (1), 307−314.
(29) He, L.; Liang, Z.; Yu, G.; Li, X.; Chen, X.; Zhou, Z.; Ren, Z. Green and Efficient Resolution of Racemic Ofloxacin Using Tartaric Acid Derivatives via Forming Cocrystal in Aqueous Solution. *Cryst. Growth Des.* **2018**, *18* (9), 5008−5020.
(30) Zhou, F.; Collard, L.; Robeyns, K.; Leyssens, T.; Shemchuk, O. l-Proline: a resolution agent able to target both enantiomers of mandelic acid: an exciting case of stoichiometry controlled chiral resolution. *Chem. Commun.* **2022**, *58* (61), 8560−8563.
(31) Guillot, M.; de Meester, J.; Huynen, S.; Collard, L.; Robeyns, K.; Riant, O.; Leyssens, T. Cocrystallization-Induced Spontaneous Deracemization: A General Thermodynamic Approach to Deracemization. *Angew. Chem., Int. Ed.* **2020**, *59* (28), 11303−11306.
(32) Songsermsawad, S.; Nalaoh, P.; Promarak, V.; Flood, A. E. Chiral Resolution of RS-Baclofen via a Novel Chiral Cocrystal of R-Baclofen and L-Mandelic Acid. *Cryst. Growth Des.* **2022**, *22* (4), 2441−2451.
(33) Gendron, F.-X.; Mahieux, J.; Sanselme, M.; Coquerel, G. Resolution of Baclofenium Hydrogenomaleate By Using Preferential Crystallization. A First Case of Complete Solid Solution at High Temperature and a Large Miscibility Gap in the Solid State. *Cryst. Growth Des.* **2019**, *19*, 4793.
(34) Huang, S.; Fitzgerald, D.; Koledoye, S. A.; Collins, S. G.; Maguire, A. R.; Lawrence, S. E. Exploring the Crystal Landscape of Mandelamide and Chiral Resolution via Cocrystallization. *Cryst. Growth Des.* **2025**, *25* (1), 1−12.
(35) Kaviani, R.; Jouyban, A.; Shayanfar, A. Chiral resolution of RS-ofloxacin through a novel diastereomeric cocrystal formation with L-

https://doi.org/10.1021/acs.cgd.5c00779
Cryst. Growth Des. 2025, 25, 6830−6836

glutamic acid by evaporative crystallization and quantification with capillary electrophoresis. *Sep. Purif. Technol.* **2025**, *354*, 129040.
(36) Buol, X.; Caro Garrido, C.; Robeyns, K.; Tumanov, N.; Collard, L.; Wouters, J.; Leyssens, T. Chiral Resolution of Mandelic Acid through Preferential Cocrystallization with Nefiracetam. *Cryst. Growth Des.* **2020**, *20* (12), 7979−7988.
(37) Harfouche, L. C.; Brandel, C.; Cartigny, Y.; Petit, S.; Coquerel, G. Resolution by Preferential Crystallization of Proxyphylline by Using Its Salicylic Acid Monohydrate Co-Crystal. *Chem. Eng. Technol.* **2020**, *43* (6), 1093−1098.
(38) Shemchuk, O.; Song, L.; Robeyns, K.; Braga, D.; Grepioni, F.; Leyssens, T. Solid-state chiral resolution mediated by stoichiometry: crystallizing etiracetam with ZnCl2. *Chem. Commun.* **2018**, *54* (77), 10890−10892.
(39) Neurohr, C.; Marchivie, M.; Lecomte, S.; Cartigny, Y.; Couvrat, N.; Sanselme, M.; Subra-Paternault, P. Naproxen−Nicotinamide Cocrystals: Racemic and Conglomerate Structures Generated by CO2 Antisolvent Crystallization. *Cryst. Growth Des.* **2015**, *15* (9), 4616−4626.
(40) Wang, L.; Wang, N.; Sui, J.; Sun, S.; Feng, Z.; Li, G.; Hao, H.; Zhou, L. Case of Chiral Resolution through Converting Two Racemic Compounds into a Conglomerate. *Cryst. Growth Des.* **2023**, *23* (8), 5641−5650.
(41) Imai, Y.; Kawaguchi, K.; Tajima, N.; Sato, T.; Kuroda, R.; Matsubara, Y. A coincident spontaneous resolution system for racemic1,1′-binaphthyl-2,2′-dicarboxylic acid and 1,2-diphenylethylenediamine induced by water. *Chem. Commun.* **2008**, No. 3, 362−364.
(42) Zhou, F.; Shemchuk, O.; Charpentier, M. D.; Matheys, C.; Collard, L.; ter Horst, J. H.; Leyssens, T. Simultaneous Chiral Resolution of Two Racemic Compounds by Preferential Cocrystallization. *Angew. Chem., Int. Ed.* **2021**, *60* (37), 20264−20268.
(43) Rapeenun, P.; Gerard, C. J. J.; Pinètre, C.; Cartigny, Y.; Tinnemans, P.; de Gelder, R.; Flood, A. E.; ter Horst, J. H. Searching for Conglomerate Cocrystals of the Racemic Compound Praziquantel. *Cryst. Growth Des.* **2024**, *24* (1), 480−490.
(44) Gerard, C. J. J.; Pinetre, C.; Cercel, H.; Charpentier, M. D.; Sanselme, M.; Couvrat, N.; Brandel, C.; Cartigny, Y.; Dupray, V.; ter Horst, J. H. Phase Diagrams of Praziquantel and Vanillic Acid Cocrystals: Racemic Compound and Conglomerate System. *Cryst. Growth Des.* **2024**, *24* (8), 3378−3387.
(45) Berry, D. J.; Seaton, C. C.; Clegg, W.; Harrington, R. W.; Coles, S. J.; Horton, P. N.; Hursthouse, M. B.; Storey, R.; Jones, W.; Friščić, T.; et al. Applying Hot-Stage Microscopy to Co-Crystal Screening: A Study of Nicotinamide with Seven Active Pharmaceutical Ingredients. *Cryst. Growth Des.* **2008**, *8* (5), 1697−1712.
(46) Springuel, G.; Norberg, B.; Robeyns, K.; Wouters, J.; Leyssens, T. Advances in Pharmaceutical Co-crystal Screening: Effective Co-crystal Screening through Structural Resemblance. *Cryst. Growth Des.* **2012**, *12* (1), 475−484.
(47) Tilborg, A.; Springuel, G.; Norberg, B.; Wouters, J.; Leyssens, T. On the influence of using a zwitterionic coformer for cocrystallization: structural focus on naproxen-proline cocrystals. *CrystEngComm* **2013**, *15* (17), 3341−3350.
(48) Tumanova, N.; Payen, R.; Springuel, G.; Norberg, B.; Robeyns, K.; Le Duff, C.; Wouters, J.; Leyssens, T. Cocrystallization out of the blue: DL-mandelic acid/ethyl-DL-mandelate cocrystal. *J. Mol. Struct.* **2017**, *1127*, 397−402.
(49) Songsermsawad, S.; Shemchuk, O.; Robeyns, K.; Zhou, F.; Flood, A. E.; Leyssens, T. Double Trouble: A Peculiar Case of Solid Solution Cocrystals Involving Two Chiral Compounds. *Cryst. Growth Des.* **2024**, *24* (7), 2977−2984.
(50) *CrysAlis*^{Pro} Version 1.171.37.35; Rigaku Oxford Diffraction.
(51) Sheldrick, G. SHELXT - Integrated space-group and crystal-structure determination. *Acta Crystallogr., Sect. A* **2015**, *71* (1), 3−8.
(52) Sheldrick, G. Crystal structure refinement with SHELXL. *Acta Crystallogr., Sect. C:Struct. Chem.* **2015**, *71* (1), 3−8.
(53) Kresse, G.; Furthmüller, J. Efficient iterative schemes for ab initio total-energy calculations using a plane-wave basis set. *Phys. Rev. B* **1996**, *54* (16), 11169−11186.
(54) Kresse, G.; Furthmüller, J. Efficiency of ab-initio total energy calculations for metals and semiconductors using a plane-wave basis set. *Comput. Mater. Sci.* **1996**, *6* (1), 15−50.
(55) Perdew, J. P.; Burke, K.; Ernzerhof, M. Generalized gradient approximation made simple. *Phys. Rev. Lett.* **1996**, *77* (18), 3865.
(56) Tkatchenko, A.; DiStasio Jr, R. A.; Car, R.; Scheffler, M. Accurate and efficient method for many-body van der Waals interactions. *Phys. Rev. Lett.* **2012**, *108* (23), 236402.
(57) Ambrosetti, A.; Reilly, A. M.; DiStasio, R. A.; Tkatchenko, A. Long-range correlation energy calculated from coupled atomic response functions. *J. Chem. Phys.* **2014**, *140* (18), 18A508.
(58) Kresse, G.; Joubert, D. From ultrasoft pseudopotentials to the projector augmented-wave method. *Phys. Rev. B* **1999**, *59* (3), 1758.
(59) Hjorth Larsen, A.; Jørgen Mortensen, J.; Blomqvist, J.; Castelli, I. E.; Christensen, R.; Dułak, M.; Friis, J.; Groves, M. N.; Hammer, B.; Hargus, C.; et al. The atomic simulation environment—a Python library for working with atoms. *J. Phys.: Condens. Matter* **2017**, *29* (27), 273002.
(60) Hoja, J.; Reilly, A. M.; Tkatchenko, A. First-principles modeling of molecular crystals: structures and stabilities, temperature and pressure. *Wiley Interdiscip. Rev.: Comput. Mol. Sci.* **2017**, *7* (1), No. e1294.
(61) Hoja, J.; Ko, H.-Y.; Neumann, M. A.; Car, R.; DiStasio Jr, R. A.; Tkatchenko, A. Reliable and practical computational description of molecular crystal polymorphs. *Sci. Adv.* **2019**, *5* (1), No. eaau3338.
(62) Chen, L.; Li, X.; Tian, T.; Yang, S.; Wang, H. Enantioseparation and mechanism study on baclofen by capillary electrophoresis and molecular modeling. *J. Pharm. Biomed. Anal.* **2023**, *229*, 115371.
(63) Strong, L. E.; Drake, D. Ionization of Aqueous Mandelic Acid: Conductance and Thermodynamics. *Proc. Indiana Acad. Sci.* **1978**, *88*, 140−148.
(64) Cutrignelli, A.; Denora, N.; Lopedota, A.; Trapani, A.; Laquintana, V.; Latrofa, A.; Trapani, G.; Liso, G. Comparative effects of some hydrophilic excipients on the rate of gabapentin and baclofen lactamization in lyophilized formulations. *Int. J. Pharm.* **2007**, *332* (1), 98−106.
(65) Hoja, J.; Tkatchenko, A. First-principles stability ranking of molecular crystal polymorphs with the DFT+MBD approach. *Faraday Discuss.* **2018**, *211* (0), 253−274.
(66) Reilly, A. M.; Tkatchenko, A. Role of dispersion interactions in the polymorphism and entropic stabilization of the aspirin crystal. *Phys. Rev. Lett.* **2014**, *113* (5), 055701.

https://doi.org/10.1021/acs.cgd.5c00779
Cryst. Growth Des. 2025, 25, 6830−6836